Microstructural Evaluation of Welded Nickel-Based Superalloy Inconel 740H After Creep Testing

KINGA A. UNOCIC,[1,3] XIANG CHEN,[2] and PETER F. TORTORELLI[2]

1.—Center for Nanophase Materials Sciences, Oak Ridge National Laboratory, Oak Ridge, USA.
2.—Materials Science and Technology Division, Oak Ridge National Laboratory, Oak Ridge, TN, USA.
3.—e-mail: unocicka@ornl.gov

Inconel 740H® alloy is considered a leading candidate for advanced ultra-supercritical steam power generation at temperatures up to 750°C and pressures up to 35 MPa. Stable alloy microstructures for extremely long-term use are needed; however, extended exposure to high temperatures and stresses can lead to microstructural instabilities when the material is joined with other alloys, thereby decreasing component lifetime. It is, therefore, critical to understand the microstructural evolution of weldments of this alloy during high-temperature and high-pressure exposures. This research specifically aims to evaluate the effects of stress and joining processes on the lifetime of Inconel 740H welded with Thermanit 263 filler metal (based on Alloy 263™). Electron microscopy techniques were used to evaluate the evolution of γ'-precipitates, grain boundary phases, grain sizes and boundary types, weldment interfaces, and other relevant microstructural characteristics resulting from long-term exposure at elevated temperatures (650–850°C) and external stresses (53–440 MPa) during creep testing. The creep strength of Inconel 740H weldments with Alloy 263 (740H/263) as a filler metal was less than that of Inconel 740H/740H base metal because of the microstructural instability of Alloy 263 at the subject creep temperatures.

INTRODUCTION

The worldwide development of advanced-ultrasupercritical (A-USC) technology is intended to help power plants generate electricity and burn less coal per megawatt-hour (meaning less coal for electricity production) while subsequently decreasing fuel cost per megawatt and decreasing emissions of CO_2. Higher operating temperatures and pressures can lead to greater efficiency of fossil-fuel powered steam boilers. A-USC conditions of temperature and pressure include steam conditions of up to 760°C and 35 MPa.[1–6] These can result in 10–12% higher efficiencies than conventional coal-fired power plants and concomitant reductions in CO_2 emission.[1,3] For these applications, the challenge becomes selecting alloys that can sustain high-temperature steam environments. These conditions rule out the potential use of ferritic and stainless steels and most solid solution–strengthened Ni-based alloys[1,7] because they do not possess the needed high-temperature mechanical properties

and thermal stability. Thus, the frontrunner alloys for these conditions are precipitation-strengthened Ni-based alloys, and there are several candidate alloys durable enough to sustain the operating conditions in A-USC power plants. Inconel 740H® and Haynes 282® are currently the leading candidates for A-USC power plants for both turbine and boiler applications. In this study, we focus on Inconel 740H. Additionally, materials joining of the materials is an important aspect of fabricating components, and the weldability of Inconel 740 and 740H with matching filler metal has previously been studied.[7] In this study, weldments of crept Inconel 740H with Thermanit 263® filler metal were evaluated.

Inconel 740H is an age-hardenable Ni-based alloy developed by Special Metals Corporation.[7] Its application is in the heavy section components in boilers and turbines.[7–10] Inconel 740H is a derivative of the original Inconel 740 but with a modified composition, particularly decreased Ti to hinder the formation of η-phase, and increased Al to improve the

stability of γ'.[7] Also, the Si level is reduced to avoid complex silicide G-phase formation. Inconel 740H is precipitation-strengthened by γ' [Ni$_3$(Ti,Al)] precipitates with L1$_2$ structure. Additionally, the microstructure contains large, blocky primary Ti–rich MC carbides with face-centered-cubic structure (fcc); fcc Cr-rich M$_{23}$C$_6$ carbides; and η-phase (Ni$_3$Ti) (750°C to 850°C). Moreover, Inconel 740H has a high fraction of grain boundaries with coincident site lattices (CSLs) that are characterized by low energy as a result of a good atomic fit. Specifically, two types of CSL (Σ3 and Σ9) boundaries are found in Inconel 740H. Thus, the presence of special grain boundaries, particularly of the Σ3 type with its high proportion of coincident sites, improves the creep resistance of the alloy.[11,12] Corrosion resistance is also an important property for A-USC applications. For superheater tubing, the alloy must resist both steam oxidation on the inside and coal ash corrosion on the fire side.[7] Because of the high Cr content (25 wt.%) in 740H, the formation of a protective Cr$_2$O$_3$ oxide layer provides long-term protection against both steam oxidation and coal-ash corrosion at high temperatures. The compositional modifications associated with Inconel 740H improved the weldability of this alloy class,[7] making it a good candidate for fabrication in heavy section weldments.[13]

Nimonic® 263 alloy, which forms the basis of the Thermanit 263 filler metal (Böhler Welding) used for the weldments in this study, is an aerospace superalloy originally developed by Rolls-Royce Ltd. in 1971 and it is a precursor for Inconel 740 and Inconel 740H. It is used in gas turbine applications because it has good oxidation resistance and attractive creep strength. It is readily fabricable with good ductility in welded assemblies compared with Nimonic 80A.[14,15] Its high Cr content improves high-temperature oxidation resistance, while a high Ti level and low Al will eventually promote the formation of η-phase (Ni$_3$Ti). In general, the microstructure of Nimonic 263 consists of fcc MC (Ti, Mo) carbides (forming at grain interiors), grain boundary fcc M$_{23}$C$_6$ (M = Cr, Mo, and Co) carbides, grain interior L1$_2$ γ' Ni$_3$(Ti,Al) precipitates, and plate-like η-phase (Ni$_3$Ti).[14,16]

In this work, creep-rupture specimens of Inconel 740H welded with Thermanit 263 were used to investigate welds and their microstructures after exposure to high temperature and stresses, to evaluate any tendency for microstructural instability under such conditions. We found a correlation between the microstructural changes in Alloy 263 welds with increasing temperature and mechanical performance.

EXPERIMENTAL PROCEDURE

A plate of Inconel 740H was welded using shielded metal arc welding, since that is one of the joining techniques being evaluated for use in A-USC

power generation plants. The Inconel 740H was welded in an annealed (1107°C for 1 h, water quench) and aged (800°C for 4 h, air quench) condition and then given a post-weld heat treatment. Thermanit 263, used as a filler metal, was procured from Böhler Welding (it is a variant of Ni-based Alloy 263). The compositions in wt.% of Inconel 740H and Alloy 263 are shown in Table I. For comparison, the composition of Inconel 740 is also included. Machined cross-weld creep-rupture specimens from a welded plate underwent post-weld heat treatment (800°C/4 h). Creep-rupture testing was conducted following the ASTM E139 standard using smooth-bar specimens (6.4-mm diameter with a 31.8-mm gauge length) at three different temperatures (650°C, 750°C, and 850°C) with five projected lifetimes (1000 h, 2500 h, 4500 h, 8000 h, and 20,000 h). Creep-rupture testing details can be found elsewhere.[17] All creep-rupture tests were conducted with constant loading until failure at the test temperature. The results were compared with the extensive ORNL database on Inconel 740/740H creep rupture from the previous A-USC boiler program.[5,6,17]

Characterization of the microstructure after creep testing involved analysis of the base (Inconel 740H) and weld (Alloy 263) metals from the stressed (gauge) section. Microstructural characterization included optical microscopy; scanning electron microscopy (SEM) using a Hitachi S4800 and a JEOL model 6500F;[18] and scanning transmission electron microscopy (S/TEM) using an FEI F200X Talos operating at 200 kV, equipped with an extreme field emission gun (X-FEG) electron source, a high-angle annular dark-field (HAADF) detector, and a Super-X EDS (energy-dispersive x-ray spectroscopy) system with four silicon-drift detectors (SDD) (Bruker XFlash 120 mm^2). Part of the microscopy was also performed on a JEOL 2200FS STEM/TEM instrument operating at 200 kV, equipped with a CEOS GmbH (Heidelberg, Germany) corrector on the illuminating lenses and an EDS system (30 mm^2 XFlash® 5030 T Bruker). TEM specimens were prepared from the polished cross sections from the weld using focus ion beam milling and an in situ lift-out method. Bulk polished specimens for optical microscopy analysis were etched with electrolyte containing 15 mL glycerol, 5 mL HNO$_3$, and 10 mL HCl.

RESULTS AND DISCUSSION

General Observations and Microstructure

Figure 1 shows an optical image of the entire weld cross section before creep testing. The weld itself was about 10 mm wide with an intact interface between the Alloy 263 weld and the base metal (Fig. 1a). Figure 1b shows higher magnification of optical images from Fig. 1 showing the interface between weld and base metal as well as the center of the weld. Evidently, Inconel 740H is characterized

Table I. Nominal composition of Inconel 740, 740H and Alloy 263 in wt.%

	Ni	Cr	Co	Ti	Al	Nb	Fe	Mo	Mn	Si	C
IN740	Bal	25	20	1.8	0.9	2.0	0.7	0.5	0.3	0.5	0.03
IN 740H	Bal	24.5	20	1.4	1.4	1.5	1.5	0.1	0.5	0.15	0.03
Alloy 263	Bal	20	20	2.2	0.6	–	0.7	5.9	0.6	0.4	0.06
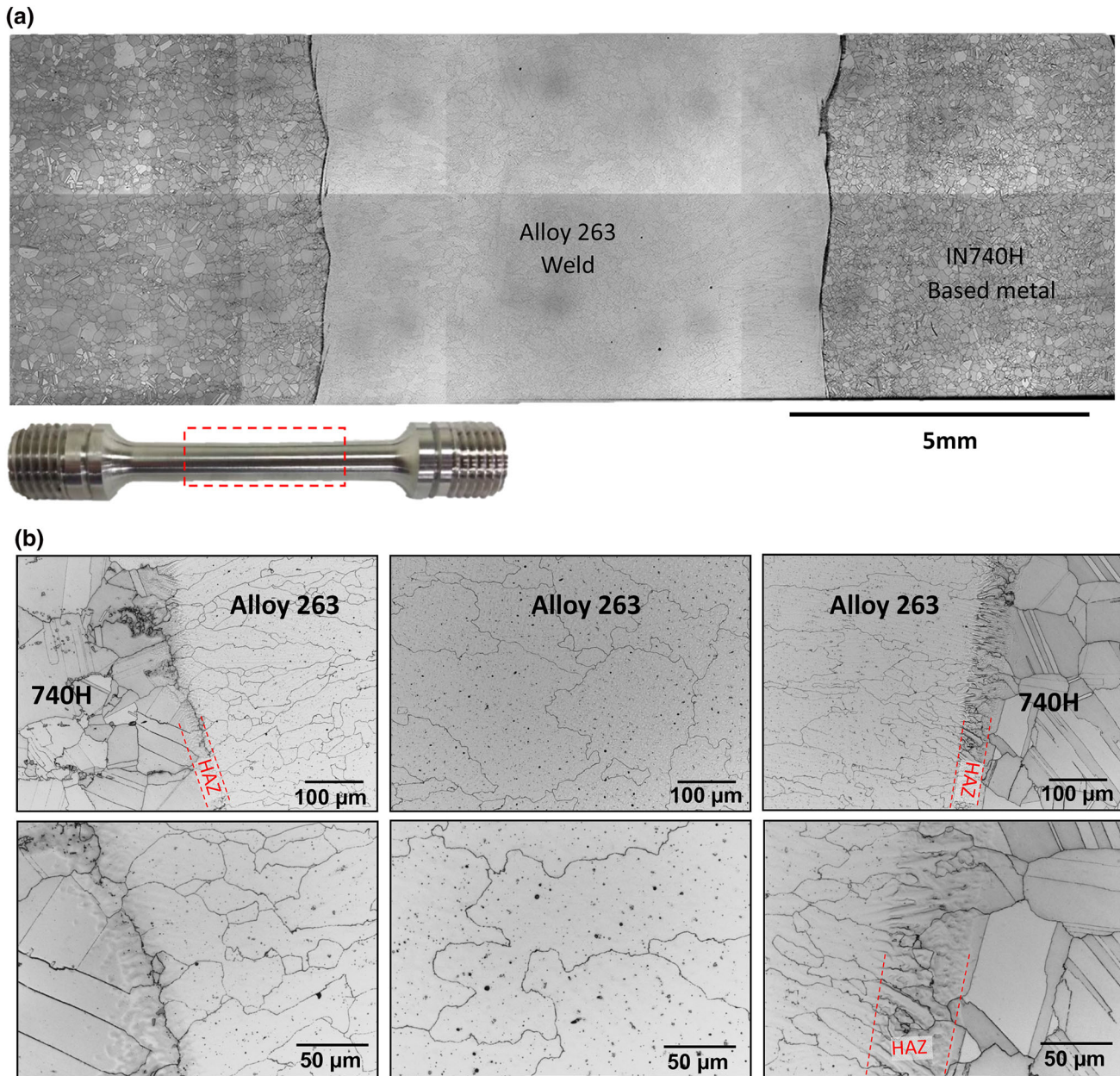
Fig. 1. Optical images showing (a) entire weld cross-section and (b) higher magnification of the center of the weld of Alloy 263 and the interface between Inconel 740H and Alloy 263 after post-weld annealing treatment before creep testing.

by smaller grains containing a number of special grain boundaries such as twins, whereas grains within the center of the weld were larger ($\sim 300\ \mu$m) with random grain boundaries and no indication of twins. The heat-affected zone (HAZ) was about 50 μm wide and was free of HAZ micro-fissures, which are often found in restrained welds of Ni-based alloys with a wide freezing range.[7] As expected, at the interface, the grains of the weld metal (Alloy 263) were elongated owing to the

solidification of the weld; whereas, at the center of the weld, less elongated grains were observed.

Fifteen specimens were creep tested at 650°C, 750°C and 850°C. Figure 2 compares the creep behavior of the cross-weld specimens of Inconel 740H base metal with that of Inconel 740H weldments with Alloy 263 filler metal. The solid symbols (triangles) indicate completed tests, and open symbols refer to the ongoing tests. The solid line is the master fitted curve from creep testing of 740H/740 base metal,[5,17] and the dashed line indicates 25% lower strength than the base metal (740H/740) stress. The creep-rupture results indicated that weldments of Inconel 740H with Alloy 263 showed shorter lifetimes than Inconel 740 and 740H specimens containing the base metal only. Also, the degree of strength reduction was dependent on the test temperature. At the testing temperatures of 650 and 750°C, the weldments were weaker by about 15% than was the Inconel 740H/740 (solid triangles were below the 740H/740 solid line); at 850°C, the creep strength was even less compared with Inconel 740H/740, considerably more than 25% less. Lower strengths are expected for Inconel 740H/ Alloy 263 welds than for Inconel 740H/740; the loss of strength is related to the respective alloy compositions (Ti and Al amount) and microstructures, as is addressed in the following sections.

Figure 3 shows polished cross sections of selected specimens after creep-rupture testing. For the three test temperatures, examples were taken at lower (Fig. 3a) and higher (Fig. 3b) applied stresses. Figure 3c shows higher magnification of the weld shown in Fig. 3a and b. All failures occurred within the weld, where formation of voids, cavities, and secondary cracks was found (Fig. 3c). Analysis of the results suggests that, for all temperatures at lower stresses, the rupture was close to the middle of the weld (Fig. 3a), with the metal/weld interface

relatively perpendicular to the load direction. However, for higher stresses, the failure was contained within the weld; but it was closer to the metal/weld interface (Fig. 3b), and the metal/weld interface was reoriented by $\sim 45°$ with respect to the loading direction.

At 650°C, in the weld (Alloy 263), γ' precipitates were finely dispersed in grain interiors; and small random grain boundary cracks perpendicular to the load direction were found. At shorter exposures (~ 2000 h), grains were not reoriented nor elongated as a result of the applied load. But after longer exposure times (~ 4000 h) saddle grain reorientation due to applied stress was observed (Supplement 1). As expected, large plate-like precipitates (η-Ni$_3$Ti phase) were not found at such low temperatures. However, higher-magnification SEM characterization of the sample tested for longer times (~ 4000 h) captured the initiation of the η-Ni$_3$Ti phase formation (Fig. 4a), which was mainly associated with the area close to carbides, particularly MC carbides (M = Mo, Ti). This finding suggests that the evolution and growth of the η-Ni$_3$Ti phase occurred, to some extent, at the expense of Ti consumption from the surrounding carbides at this temperature.[19] The average size of the Mo, Ti carbides for this temperature was 0.82 ± 0.07 μm. They were randomly distributed within grain interiors, with some also found at the grain boundaries. The sizes of the MC carbides measured after each testing condition are summarized in Fig. 5a. Grain boundaries were mainly decorated with M$_{23}$C$_6$ (M = Cr, Mo). At higher stress (440 MPa/650°C), grains were more elongated with random grain boundary cracks (Fig. 3b).

At 750°C, at both lower (189 MPa) and higher (219 MPa) stresses, the grains were elongated and reoriented along 45° to the loading direction, compared with the 650°C specimens. Some grains near the fracture surface were still not elongated. Grain boundary cracks, small voids, and cavities were present at grain boundaries (Fig. 4b). Additionally, a phase change to η-Ni$_3$Ti phase was more readily observed than was the case at 650°C. The average size of the η-Ni$_3$Ti phase was 2.17 μm ± 0.7 μm (Fig. 5b); it appeared near MC carbides forming a local Widmanstätten pattern (Fig. 4b). The average size of the Mo, Ti carbides was 0.67 μm ± 0.02 μm (Fig. 5a), which slightly decreased when compared with the carbides present at 650°C.

At 850°C, cavities, voids, and small and large random grain boundary cracks aligned perpendicular to the loading direction were observed (Fig. 4c, d). Additionally, at higher applied stress (84 MPa), large cracks penetrated the grain boundaries; the cracks aligned close to 45° to the applied load with a few cracks propagating to the base metal across the interface (Fig. 7c). After a shorter exposure time (~ 800 h), grains were slightly elongated near the fracture surface. However, after longer exposure and lower stresses, grains seemed to be more
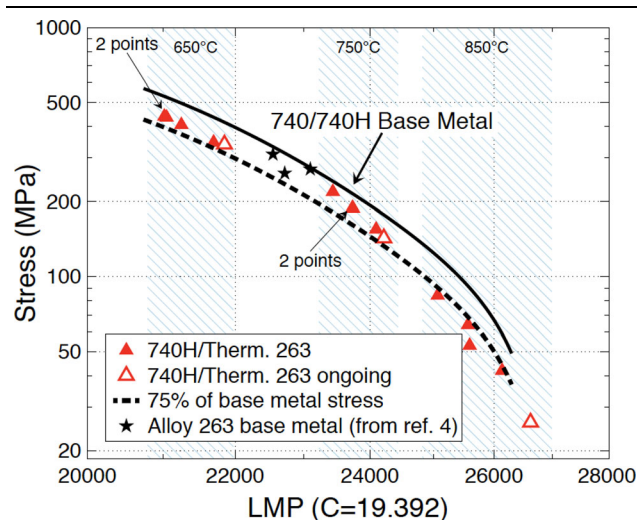

Fig. 2. Comparison of the Larson-Miller parameter of 740H/Alloy 263 cross-weld with 740H/740 base metal and the base-metal data for Alloy 263 adapted from Viswanathan et al.[4]
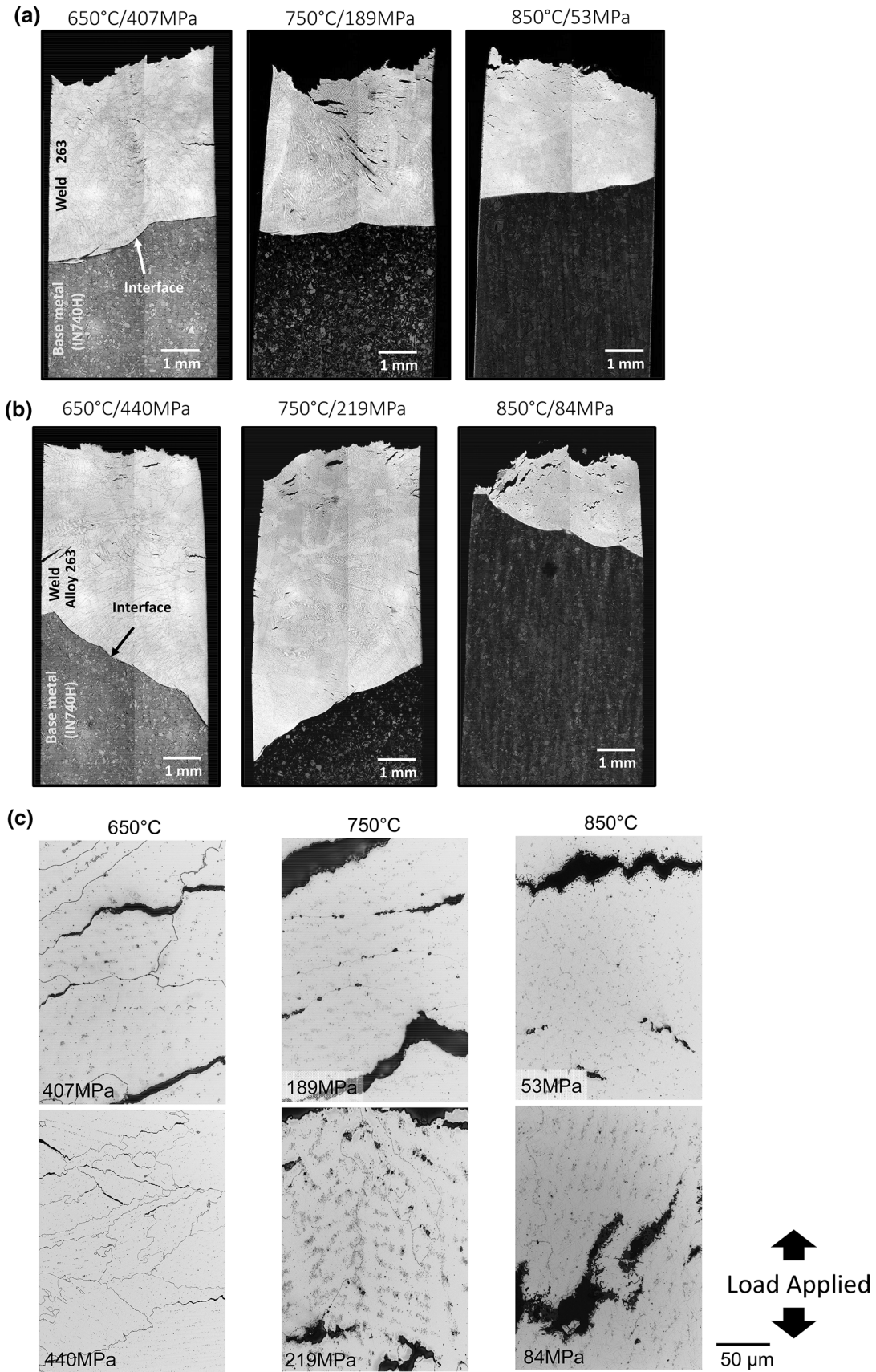
Fig. 3. Optical images showing polished cross section of the creep-rupture specimens after a failure for three different temperatures for (a) lower stresses and (b) higher stresses. (c) Higher-magnification images from the weld section for all the conditions.
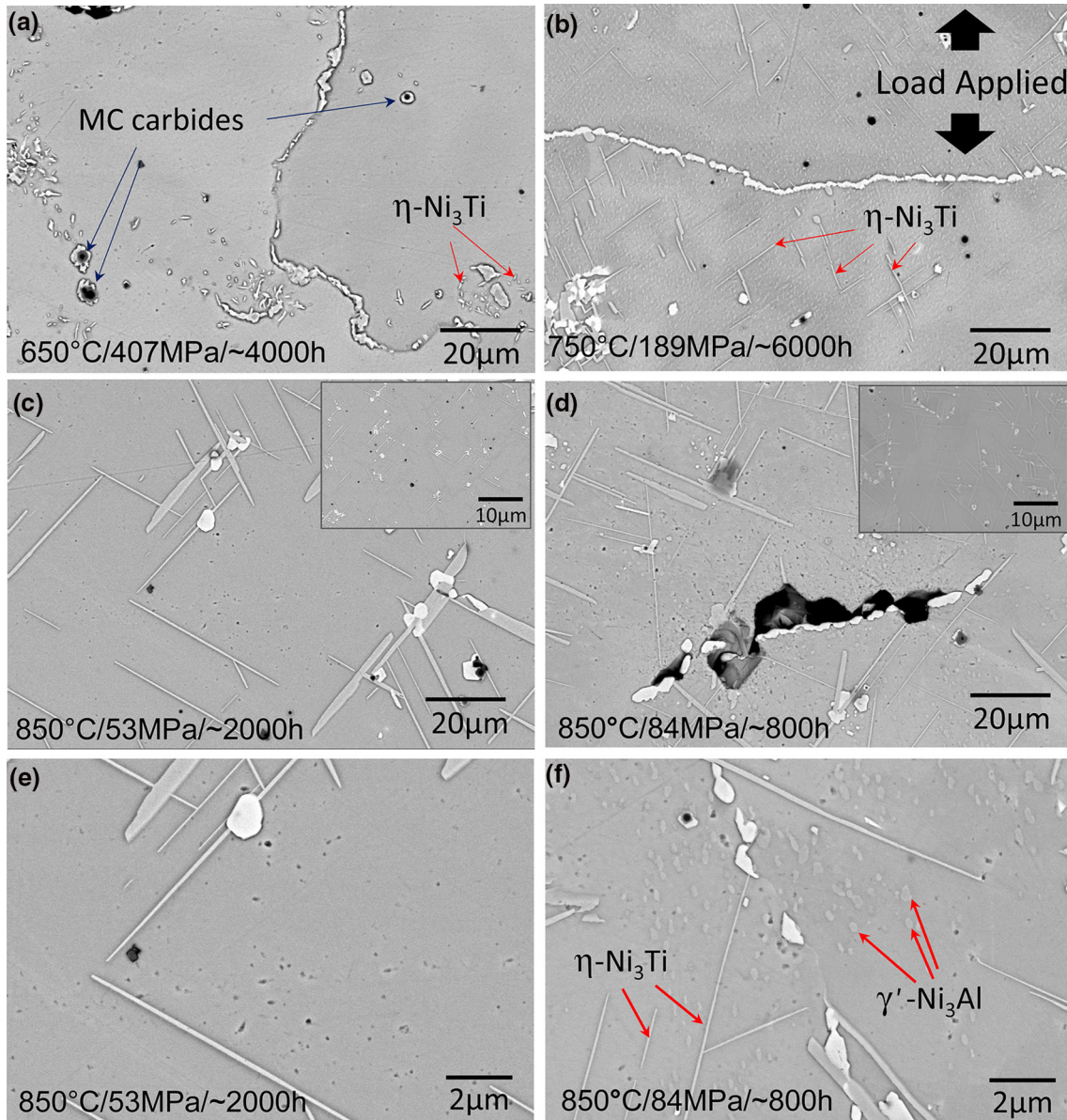
Fig. 4. Backscattered electron (BSE) images showing Alloy 263 from the gauge region for (a) 650°C/407 MPa/∼ 4000 h, (b) 750°C/189 MPa/ ∼ 6000 h, (c) 850°C/53 MPa/∼ 2000 h, and (d) 850°C/84 MPa/∼ 800 h. Higher-magnification images showing microstructure for (e) 850°C/ 53 MPa/∼ 2000 h and (f) 850°C/84 MPa/∼ 800 h conditions.

equiaxed, as shown by electron backscatter diffraction (EBSD) (see Supplementary Fig. S1). Already after ∼ 800 h, a high volume fraction of η-Ni$_3$Ti phase plates was found with an average size of 6.51 μm $\pm$ 2.3 μm; they were arranged in a strong Widmanstätten pattern. The average size of η-Ni$_3$Ti phase plates formed at 850°C was 7.17 μm $\pm$ 0.8 μm; they were much larger than those found at 750°C (2.18 μm $\pm$ 0.8 μm) (Fig. 4c, d). A summary of η-Ni$_3$Ti phase plate average size measurements for both temperatures is shown in Fig. 5b. Additionally, the sizes of Mo, Ti carbides decreased (Fig. 5a).

In the areas between η-Ni$_3$Ti phases, areas with large γ' phase were found, but their number decreased (Fig. 4f) compared with samples exposed at lower temperatures. Part of the disappearance of the γ' phase is related to Ti consumption from the γ' phase by the growing η-Ni$_3$Ti phase. An example of the γ' phase with EDS elemental maps of Al and Ti is shown in Fig. 6. The bright field-STEM image also shows η-Ni$_3$Ti phase plates clearly outlined by Ni and Ti elemental maps. Further, the grain boundary Mo, Cr-carbide shows enrichment in Si. Finally, coarsening of the γ' phase was observed in the base metal (Inconel 740H). Overall, at 850°C, the growth of η-Ni$_3$Ti phase plates was at the expense of consumption of Ti from both Mo, Ti carbides and the γ' phase (Ni$_3$Al,Ti).
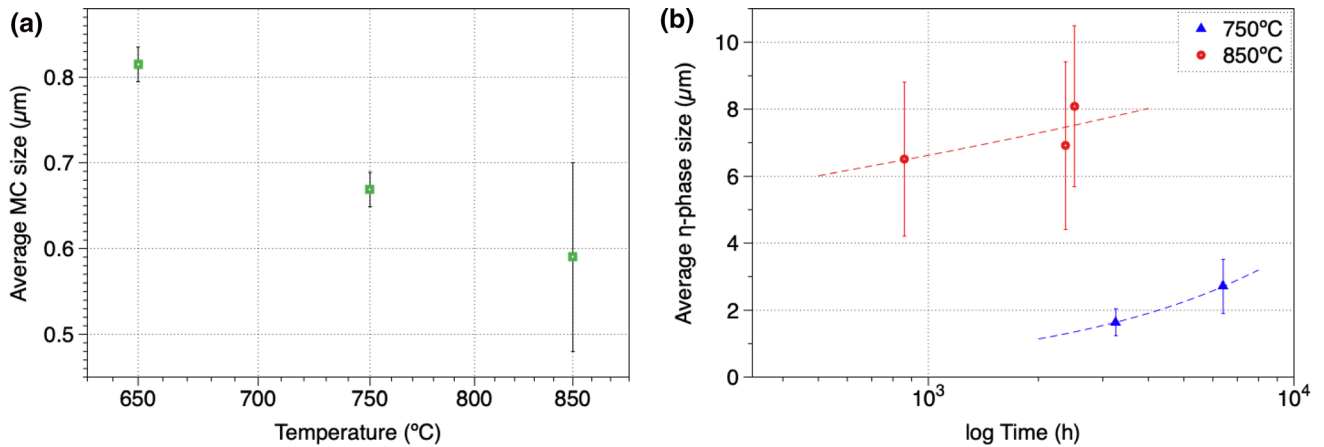
Fig. 5. (a) Average size of Mo, Ti carbides measured for different temperatures. (b) Average size of η-Ni$_3$Ti phase.
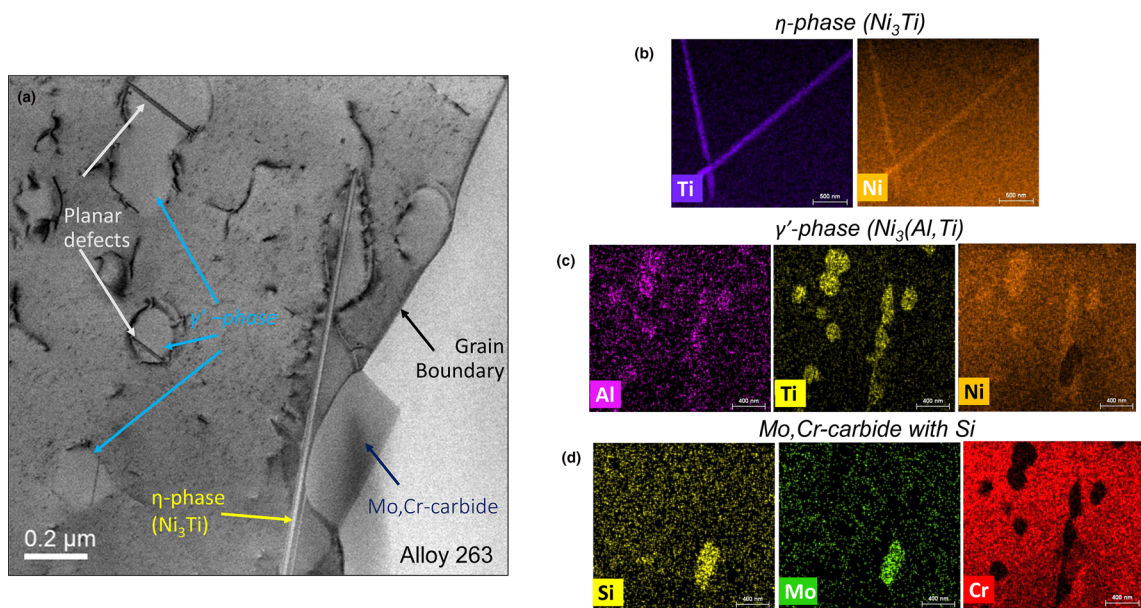

Fig. 6. (a) Bright field–STEM image showing microstructure of Alloy 263 after creep-rupture testing (850°C/84 MPa/$\sim$ 860 h) with EDS elemental maps showing existence of three different phases: (b) η-phase (Ni$_3$Ti), (c) γ'-phase [Ni$_3$(Al,Ti)], and (d) Mo-carbide.

Figure 7 shows an example of the interface between the base metal and the weld. At 650°C and 750°C, for both low and high stresses, the interface remained intact. At 850°C, when the interfaces at two different stress levels are compared, the interface at lower stress (53 MPa) remains intact (Fig. 7b), whereas the specimen exposed to higher stress (84 MPa) shows advanced cracks along grain boundaries, almost reaching the base metal/weld interface (Fig. 7c).

Oxidation

The oxidation behavior of the welds (Alloy 263) exposed to air at 650–850°C under stress was also studied (Fig. 8). As expected, the extent of oxidation evolved with increasing temperature. The microstructure and phase composition of oxide scale were analyzed by SEM and EDS (Fig. 9). After exposure at 650°C (Fig. 9a), a thin double oxide layer ($\sim$ 0.5 μm) formed with negligible internal oxidation. The outer oxide layer was mostly spinel enriched in Ti, Ni, and Cr, beneath which a thin silica inner layer was present. The oxide/metal interface was enriched in Mo. A thicker surface oxide layer was found on the sample tested at 750°C ($\sim$ 2 μm) with more extensive internal oxidation of about 10 μm. The EDS elemental maps (not shown here) revealed a three-layer structure. The outer oxide layer consisted of Ti and Cr with some incorporation of Al, while the middle layer was mainly chromia (Cr$_2$O$_3$), beneath which a silica inner layer enriched in Ti was found. Similar to the results at a lower temperature (650°C), there was some Mo enrichment just beneath the oxide layer.

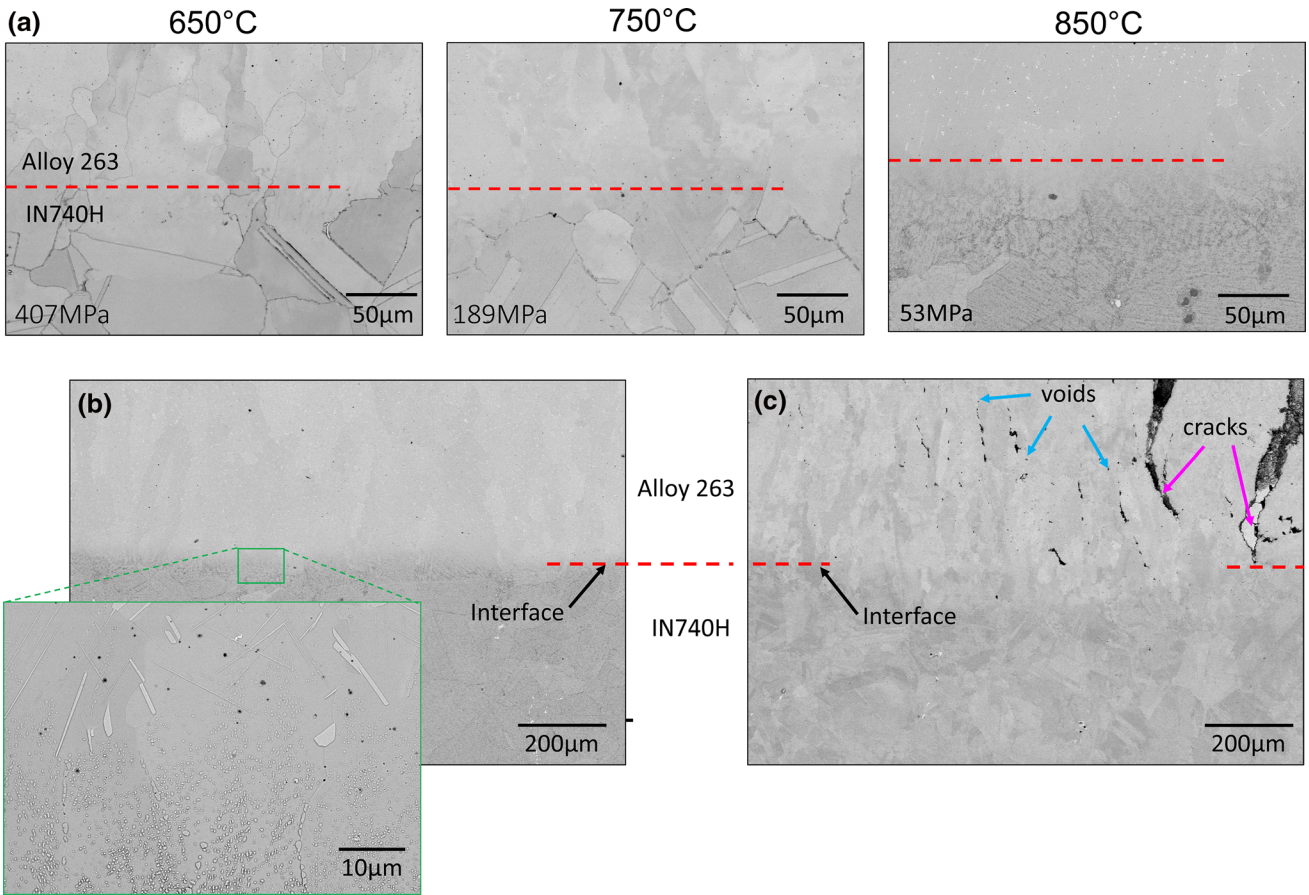At 850°C, even though the exposure time was shorter than at 750°C, the oxide was much thicker,

Fig. 7. (a) BSE images showing interface after creep-rupture test at 650, 750, and 850°C. Higher-magnification BSE images showing interface after creep-rupture test at 850°C for different stress levels: (b) 53 MPa/∼ 2000 h and (c) 84 MPa/∼ 800 h.
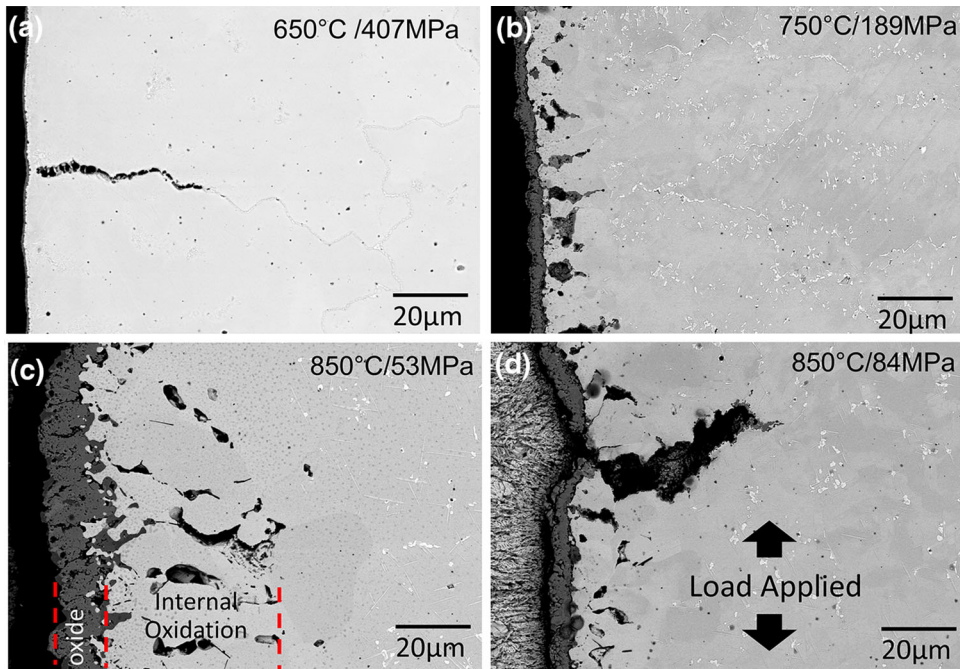

Fig. 8. BSE images showing exposed surface after creep-rupture test under different conditions: (a) 650°C 407 MPa/∼ 4000 h, (b) 750°C 189 MPa/∼ 6000 h, (c) 850°C 53 MPa/∼ 2000 h, and (d) 850°C 84 MPa/∼ 800 h.
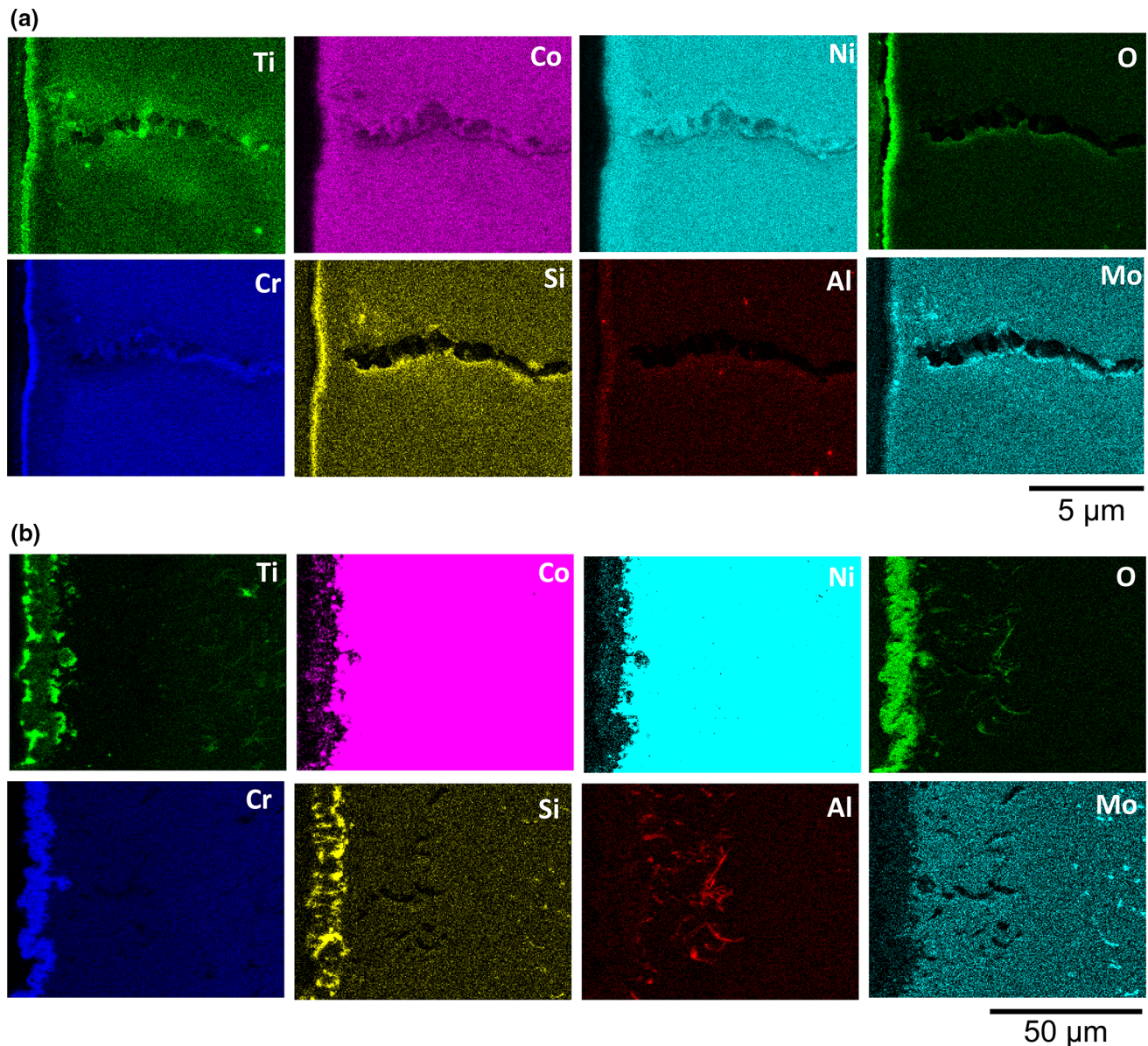
(a)

(b)

Fig. 9. EDS elemental maps for (a) 650°C/407 MPa/∼ 4000 h and (b) 850°C/53 MPa/∼ 2000 h.

15 μm. The EDS elemental maps identified a three-layer structure (Fig. 9b). The outer layer was enriched in Ti-oxide particles, the intermediate layer included mainly Cr_2O_3, and the inner layer was enriched again in Ti- and Si-oxide particles. There was no continuous silica layer. Also, at this temperature, there was no Mo enrichment beneath the oxide layer. Oxidation behavior of Nimonic 263 alloy exposed up to 1000 h to deaerated supercritical water at 600–700°C under 25 MPa was studied by Zhu et al.[20] The work showed a complex oxide structure formed on the surface of Nimonic 263, including an outer layer of Ni-Fe/Ni-Cr spinel oxide, Ni/Co hydroxide, and TiO_2 and an inner layer of a mixture of $NiCr_2O_4$ and Cr_2O_3; the innermost layer was made up of Cr_2O_3. Interestingly, at 600°C, the authors found a MoO_3 layer, which disappeared

with increasing temperature. This finding suggests that enrichment of Mo at the metal/oxide interface in our work might actually be related to the formation of the MoO_3 layer, which requires additional characterization for further confirmation. Nevertheless, this layer vanishes with exposure to higher temperatures, which is similar to the observation by Zhu et al. In summary, the complexity of the morphology and thickness of the oxide layer grows with increasing temperature.

Deformation Mechanism

The deformation mechanism in γ'-strengthened Ni-based superalloys has been studied in great detail by a number of researchers.[21–23] In general, the deformation mechanism changes with

(a) 750°C/189MPa/~6000h

(b) 750°C/219MPa/ ~3000h
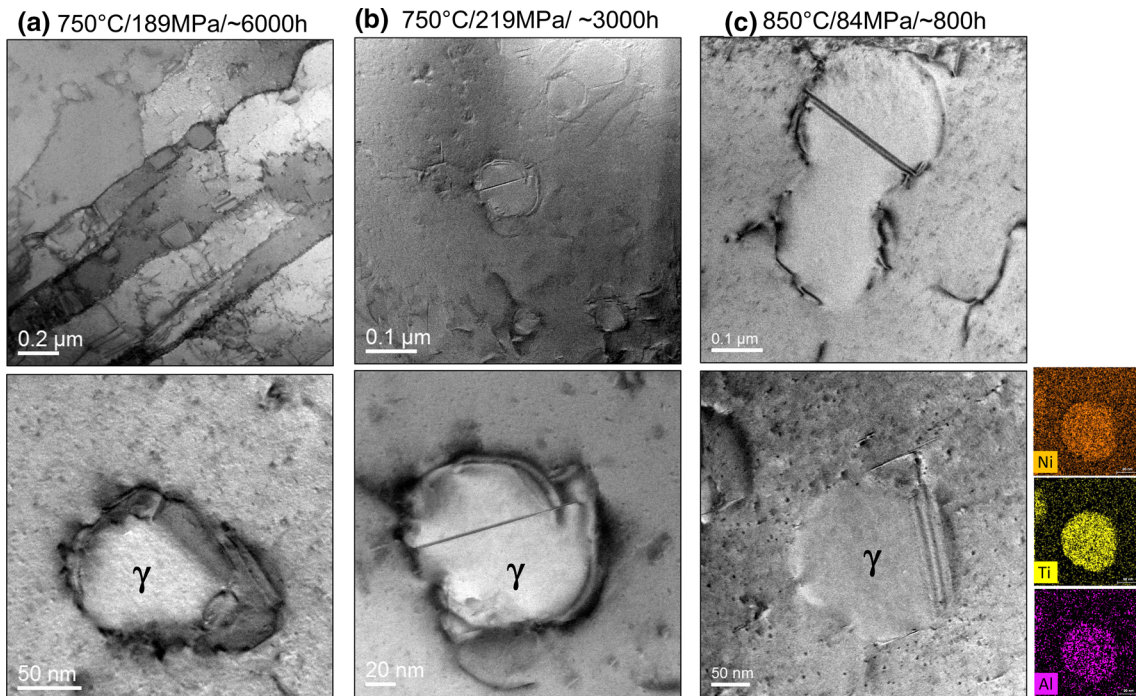
(c) 850°C/84MPa/~800h

Fig. 10. Bright field–STEM images of Alloy 263 showing examples of the microstructure from the stressed region tested at (a) 750°C/189 MPa with creep lifetime of ∼ 6000 h, (b) 750°C/219 MPa with creep lifetime of ∼ 3000 h, and (c) 850°C/84 MPa with creep lifetime of ∼ 800 h with EDS elemental maps confirming γ' phase.

increasing γ' precipitates size.[21, 24] Small γ' precipitates undergo cutting by weakly paired dislocations to strongly paired dislocations, while large γ' precipitates are bypassed by Orowan looping of dislocations. The size of γ' precipitates in the weld metal (Alloy 263) at 750°C was ∼ 120 nm after testing for ∼ 3200 h and ∼ 250 nm after testing for ∼ 6400 h; whereas at 850°C, the size of γ' precipitates was ∼ 100 nm after ∼ 800 h with reduced number density due to the formation of η-Ni_3Ti phase formation. At both temperatures, dislocation cutting was found mainly at shorter exposure times (Figs. 10b and c), indicating the resistance of γ' precipitates to the deformation. This finding further implies that even though γ' precipitates were coarsening and decreasing in number density with high-temperature exposure (850°C) (Fig. 10c), they still acted as the deformation barrier. At longer testing times (∼ 6000 h) at 750°C, dislocation pinning by γ' precipitates was found, with limited γ' precipitates being sheared. A high dislocation network was also found in the matrix between η-Ni_3Ti phases.

Overall, the γ' precipitates in the weld metal (Alloy 263) were less stable than γ' precipitates in Inconel 740H because of the lower Al to Ti ratio, which subsequently promoted formation of η-Ni_3Ti. Therefore, the weld appeared to be the weakest point for the Inconel 740H joined with a filler metal of Alloy 263. This finding supports the creep results, explaining why the failure occurred in the weld metal and the lower creep strengths for Inconel 740H/Alloy 263 weldments compared with the Inconel 740H/740 base metal. Some comparable creep-rupture data for base-metal Alloy 263 (at 700°C)[4] are included in Fig. 2. The inclusion of these points indicates consistency with the present data for the weldments made with Alloy 263 filler metal,which show a reduction in creep resistance relative to the Inconel 740/740H base metal. This research shows that Inconel 740H/Alloy 263 weldments are suitable for operation at lower operating temperatures less than about 750°C.

CONCLUSION

Inconel 740H welded with an Alloy 263 filler metal by shielded metal arc welding was investigated after creep testing at 650°C, 750°C and 850°C. All creep failures occurred within the weld region, with intergranular failure and cracks propagated along grain boundaries. No cracks were found in the Inconel 740H base metal. The creep strength of Inconel 740H weldments with Alloy 263 filler metal was less than that of Inconel 740H base metal/ Inconel 740 because of the inferior microstructural stability of Alloy 263 at elevated temperature. Evident microstructural changes were observed in Alloy 263 tested at 850°C, with a strong Widmanstätten pattern of η-Ni_3Ti phase at the expense of Mo, Ti carbides and γ' phase (Ni_3Al,Ti). The oxidation of Alloy 263 advanced with exposure temperature.

ACKNOWLEDGEMENTS

ELECTRONIC SUPPLEMENTARY MATERIAL

The online version of this article (https://doi.org/10.1007/s11837-020-04119-2) contains supplementary material, which is available to authorized users.

REFERENCES

1. J. Shingledecker, R. Purgert, and P. Rawls, *Advances in Materials Technology for Fossil Power Plants*, ed. D. Gandy and J. Shingledecker (Materials Park,OH: ASMInt., 2014), p. 41.
2. P.S. Weitzel, J.M. Tanzosh, B. Boring, N. Okita, T. Takahashi, N, Ishikawa in *Advanced Ultra-Supercritical Power Plant (700 to 760°C), Design for Indian Coal*, Babcock & Wilcox Power Generation Group, Inc. Barberton, Ohio, USA, Power-Gen Asia, October 3–5, 2012 Bangkok, Thailand, Technical Paper No. BR-1884 1 (2012).
3. R. Viswanathan, J.F. Henry, J. Tanzosh, G. Stanko, J. Shingledecker, B. Vitalis, and R. Purgert, *J. Mater. Eng. Perform.* 14, 281 (2005).
4. A. Klenk and K. Maile, *Advances in Materials Technology for Fossil Power Plants*, ed. D. Gandy and J. Shingledecker (Materials Park: ASM Int., 2014), pp. 155–166.
5. P.F. Tortorelli, K.A. Unocic, H. Wang, M.L. Santella, and J.P. Shingledecker, *Advances in Materials Technology for Fossil Power Plants*, ed. D. Gandy and J. Shingledecker (Materials Park: ASM Int., 2014), p. 131.
6. P.F. Tortorelli, H. Wang, K.A. Unocic, M. L. Santella, J.P. Shingledecker, and V. Cedro, III, in *Proceedings of ASME Symposium on Elevated Temperature Application of Materials for Fossil, Nuclear, and Petrochemical Industries* (New York: ASME, 2014), ASME Paper ETS2014-1003 (2014).
7. S.J. Patel, J.J. de Barbadillo, B.A. Baker, and R.D. Gollihue, *Procedia Eng.* 55, 246 (2013).
8. G.D. Smith, H.W. Sizek, in *Paper 00256, presented at the NACE Annual Conference Corrosion 2000*, Orlando FL, March 26–31 (2000).
9. R.J. Smith, B.A. Baker, G.D. Smith, Nickel alloys for the next generation of advanced steam boilers, in *VGB Materials and Quality Assurance Conference*, March 10–11, Dortmund, Germany (2004).
10. J. de Barbadillo, B.A. Baker, L. Klingensmith, S.J. Patel, Nickel alloy development and use in USC boilers, in *Symposium on Advanced Power Plant Heat Resistant Alloys*, SPERI, Shanghai (2009).
11. G.S. Was, V. Thaveeprungsriporn, and D.C. Crawford, *JOM* 50, 44 (1998).
12. T. Watanabe, *Mater. Sci. Eng., A* A166, 11 (1993).
13. J.A. Siefert, J.M. Tanzosh, J.E. Ramirez, Weldability of INCONEL alloy 740, in *Proceedings of 6th International Conference on Advances in Materials Technology for Fossil Power Plants*; EPRI, Santa Fe, (2010).
14. J.-C. Zhao, V. Ravikumar, and A.M. Beltran, *Metall. Mat. Trans. A* 32A, 1271 (2001).
15. V. Ratna and D.S. Sarma, *Scr. Metall. Mater.* 29, 467 (1993).
16. B. Hicks, M. Heap: Report No. B48749, Lucas Gas Turbine Equipment Ltd., Materials Laboratory, Burnley, September 25 (1968).
17. J.P. Shingledecker and G.M. Pharr, *Mater. Metall. Trans. A* 43A, 1902 (2012).
18. K.A. Unocic, J.P. Shingledecker, and P.F. Tortorelli, *JOM* 66, 2535 (2014).
19. B.G. Choi, I.S. Kim, D.H. Kim, S.M. Seo, C.Y. Jo, *Superalloy 2004*, in K.A. Green, T.M. Pollock, H. Harada, TMS (The Minerals, Metals & Materials Society), 2004 T.E. Howson, R.C. Reed, J.J. Schirra, S, Walston (2004), p. 163.
20. Z. Zhu, H. Xu, H.I. Khan, and N. Zhang, *Corros. Eng. Sci. Technol.* 53, 617 (2018).
21. R.R. Unocic, N. Zhou, L. Kovarik, C. Shen, Y. Wang, and M.J. Mills, *Acta Mater.* 59, 7325 (2011).
22. T.M. Smith, R.R. Unocic, H. Deutchman, and M.J. Mills, *Mater. High Temp.* 33, 372 (2016).
23. L. Kovarik, R.R. Unocic, and M.J. Mills, *Prog. Mater Sci.* 54, 839 (2009).
24. M. Preuss, J.Q. da Fonseca, B. Grant, E. Knoche, R. Moat, M. Daymond, *Superalloys 2008*, TMS (the Minerals, Metals and Materials Society) (2008), p. 405.